PCCP

PAPER

View Article Online
View Journal | View Issue

Cite this: *Phys. Chem. Chem. Phys.*, 2022, **24**, 15920

New structural insights into the stability of $Au_{22}(SR)_{16}$ nanocluster under ring model guidance†

Wenhua Han,[a] Endong Wang*[bc] and Wen Wu Xu *[a]

Received 26th January 2022,
Accepted 13th June 2022

DOI: 10.1039/d2cp00421f

rsc.li/pccp

This study presents thorough structural insights into the stability of crystallized $Au_{22}(SAdm)_{16}$ (HSAdm = 1-adamantanethiol) nanocluster. With the recently developed Ring Model for describing the interaction between inner gold cores and outer protecting ligands in thiolate-protected gold nanoclusters, the experimental spontaneous transformation from the crystallized $Au_{22}(SAdm)_{16}$ to $Au_{21}(SAdm)_{15}$ could be well understood as structurally unfavorable for the current $Au_{22}(SAdm)_{16}$ and could also be attributed to the weaker aurophilic interaction between the inner Au_4 core and the surrounding rings in $Au_{22}(SAdm)_{16}$ over that in $Au_{21}(SAdm)_{15}$. Furthermore, with the Ring Model and the grand unified model, two new $Au_{22}(SCH_3)_{16}$ isomers with evident lower energies, higher HOMO–LUMO gaps as well as distinct optical properties over the available crystallized isomer were obtained. This study deepens the current knowledge on the structure of the $Au_{22}(SR)_{16}$ cluster from a new structural point of view and also confirms the validity as well as practicability of the Ring Model in understanding and predicting the stable structures of thiolate-protected gold nanoclusters.

Introduction

Understanding the structural stability of thiolate-protected gold nanoclusters is still a challenging task.[1–4] Although numerous X-ray crystallography gold nanoclusters show high stability,[5–8] several with low thermostability were also observed. For example, the experimentally crystallized $Au_{38}(PET)_{24}$ (referred as Au_{38T}, PET = SC_2H_4Ph) nanoclusters can irreversibly transform to their another crystallized isomer $Au_{38}(PET)_{24}$ (referred as Au_{38Q}) at 50 °C in toluene, indicating the low thermostablity of Au_{38T} with respect to Au_{38Q}.[9] Besides, in principle, the 18-electron closed-shell $Au_{44}(2,4\text{-DMBT})_{26}$ (2,4-DMBTH = 2,4-dimethylbenzenethiol) is expected to be more stable than 16-electron $Au_{44}(TBBT)_{28}$ (TBBTH = 4-*tert*-butylbenzenelthiol).[10] Dynamic UV/vis/NIR spectra confirms that $Au_{44}(2,4\text{-DMBT})_{26}$ can transform to other gold nanoclusters under 80 °C. Under the same conditions, similar transformation was not observed for $Au_{44}(TBBT)_{28}$, which indicates that $Au_{44}(2,4\text{-DMBT})_{26}$ is actually less thermostable than $Au_{44}(TBBT)_{28}$ under 80 °C.[10] In addition, $Au_{22}(SAdm)_{16}$ (SAdm = 1-adamantanethiol) was recently found to be metastable in a solution and can spontaneously transform into $Au_{21}(SAdm)_{15}$.[11,12] These structural alternations clearly show that some crystallized thiolate-protected gold nanoclusters with low thermostability do exist. However, the structural insights on the geometrical transformation of these crystallized structures, and if there exists a more stable isomer, are yet to be unravelled.

Over the past decades, this field has seen tremendous progresses.[13–20] Several models including divide and protect concept,[13] superatom complex model,[21] superatom network model,[22] super valence bond model,[23] polyhedra method,[24] inherent structure rule,[25] grand unified model (GUM)[26] as well as Ring model[27] have been developed to gain a better understanding of the stabilities of thiolate-protected gold nanoclusters. Among them, the Ring model was recently developed to describe the interfacial interaction between the inner gold cores and the outer protecting motifs of thiolate-protected gold nanoclusters. Several thiolate-protected clusters have been predicted *via* the Ring model, which demonstrates the usefulness in understanding the structural characters of ligand clusters.[28,29] In the Ring model, thiolate-protected gold nanoclusters can be decomposed into several fusing or interlocking $[Au_q(SR)_p]$ (q = 4–8, 10, 12, and $0 \leq p \leq q$) rings. With the Ring model, this study presents new structural insights into

[a] *Department of Physics, School of Physical Science and Technology, Ningbo University, Ningbo, 315211, China. E-mail: xuwenwu@nbu.edu.cn*
[b] *School of Chemistry and Chemical Engineering, Liaoning Normal University, Dalian, 116029, China. E-mail: edwang@lnnu.edu.cn*
[c] *State Key Laboratory of Molecular Reaction Dynamics, Dalian Institute of Chemical Physics, Chinese Academy of Sciences, Dalian, 116023, China*

† Electronic supplementary information (ESI) available: Cartesian coordinates of two predicted $Au_{22}(SCH_3)_{16}$ isomers included. See DOI: **https://doi.org/10.1039/d2cp00421f**

the less thermostability of crystallized $Au_{22}(SAdm)_{16}$ with respect to the $Au_{21}(SAdm)_{15}$ nanocluster. Furthermore, another two isomeric structures of $Au_{22}(SR)_{16}$ (R = CH_3) were obtained, which own lower relative energies and higher HOMO–LUMO gaps over the available crystallized structure.

Results and discussion

Structural understanding of $Au_{22}(SR)_{16}$ *via* the Ring model and GUM model

We first focused on the structural analysis of crystallized $Au_{22}(SR)_{16}$ and $Au_{21}(SR)_{15}$ (R = SAdm) nanoclusters in a straightforward manner following GUM. As shown in Fig. 1, GUM suggests that both clusters own one green-colored $Au_4(2e)$ elementary blocks and two blue-colored $Au_3(2e)$ elementary blocks as the kernel. Through the proper alignments of the core and the outer ligands, both $Au_{22}(SR)_{16}$ and $Au_{21}(SR)_{15}$ have one $Au_{12}(SR)_9$ part, which is made up of a Au_4 block in green background and $Au_8(SR)_9$ ligand. Upon removing this $Au_{12}(SR)_9$ part from $Au_{21}(SR)_{15}$, a $Au_9(SR)_6$ cage can be seen, as shown in Fig. 1(a). Similarly, for $Au_{22}(SR)_{16}$, a $Au_{10}(SR)_7$ cage can be observed, as given in Fig. 1(b). Therefore, Fig. 1 shows that the main structural difference between crystallized $Au_{22}(SR)_{16}$ and $Au_{21}(SR)_{15}$ lies in the aforementioned two different sized cages, *i.e.* $Au_9(SR)_6$ cage for $Au_{21}(SR)_{15}$ *vs.* $Au_{10}(SR)_7$ cage for $Au_{22}(SR)_{16}$.

With the Ring model, further analysis of the main structural difference between the $Au_9(SR)_6$ cage and the $Au_{10}(SR)_7$ cage was performed, as shown in Fig. 2. The $Au_9(SR)_6$ cage can be viewed as three rings $[Au_7(SR)_5]$, $[Au_6(SR)_4]$, and $[Au_5(SR)_3]$ fusing together (Fig. 2(a)). The $Au_{10}(SR)_7$ cage can be viewed as three rings $[Au_8(SR)_6]$, $[Au_7(SR)_5]$, and $[Au_5(SR)_3]$ fusing together (Fig. 2(b)). Therefore, the difference between the $Au_9(SR)_6$ cage of $Au_{21}(SR)_{15}$ and the $Au_{10}(SR)_7$ cage of $Au_{22}(SR)_{16}$ can be ascribed to the different rings fusing together.

With the increment of the radii of the ring, the Ring model suggests that the ring should properly match with the structures of the within this ring to maximize the interaction between the central structure and the outer ring.[27] Summarized from the available crystal structures, the Ring model suggests that there should be one gold atom in the centre of the $[Au_5(SR)_q]$ ($1 \leq q < 5$) ring.[27] For the $[Au_6(SR)_q]$ ($0 \leq q \leq 6$) ring, one gold atom or one triangular Au_3 should locate at the centre of the ring.[27] For the $[Au_7(SR)_q]$ ($q = 4$ and 5) ring, there is one tetrahedral Au_4 located at the centre of the ring.[27] For the $[Au_8(SR)_q]$ ($q = 4$ and 8) ring, there should be two tetrahedral Au_4 located at the centre of the rings.[27]

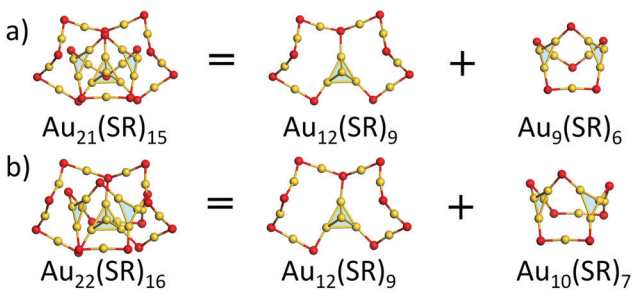

Fig. 1 Geometric decompositions of (a) $Au_{21}(SR)_{15}$ and (b) $Au_{22}(SR)_{16}$ (R = SAdm). Au: yellow; S: red. The R groups are omitted for clarity.

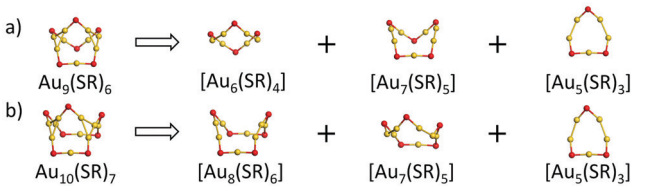

Fig. 2 Ring model-driven structural decomposition of (a) the $[Au_9(SR)_6]$ ring of $Au_{21}(SR)_{15}$ and (b) $[Au_{10}(SR)_7]$ ring of $Au_{22}(SR)_{16}$ into different rings. Au: yellow; S: red. The R groups are omitted for clarity.

Based on the structural analysis of Fig. 1 and 2, special attention should be paid to the structural configurations of the $Au_9(SR)_6$ cage of $Au_{21}(SR)_{15}$ and $Au_{10}(SR)_7$ cage of $Au_{22}(SR)_{16}$ with the ring model. As given in Fig. 3, it can be found that the $Au_9(SR)_6$ cage of the $Au_{21}(SR)_{15}$ cluster one gold atom is located at the centre of $[Au_6(SR)_4]$ ring, which satisfies the ring model. However, for the $Au_{10}(SR)_7$ cage of the $Au_{22}(SR)_{16}$ cluster, there is only one tetrahedral Au_4 located at the centre of the $[Au_8(SR)_6]$ ring, which conflicts with the Ring model, namely, two Au_4 should exist within $[Au_8(SR)_8]$ ring, as given in Table 1. Therefore, the experimental result could be ascribed to the confliction with the Ring model for the structural configuration in $Au_{22}(SR)_{16}$. For the $[Au_7(SR)_5]$ ring and $[Au_5(SR)_3]$ ring of both clusters, there is one tetrahedral Au_4 located at the centre of the $[Au_7(SR)_5]$ ring and one gold atom located below the centre of the $[Au_5(SR)_3]$ ring, as given in Fig. S2 (ESI†), which is in accordance with the Ring model.

In addition, the average distance between the gold atoms in tetrahedral Au_4 and the gold atoms of three rings in the $Au_9(SR)_6$ cage in $Au_{21}(SR)_{15}$ (Fig. 2a) and the $Au_{10}(SR)_7$ cage in $Au_{22}(SR)_{16}$ (Fig. 2b) are also presented in Table 2. It can be found that the average Au–Au distances between Au_4 and $Au_{10}(SR)_7$ cage in $Au_{22}(SR)_{16}$ are larger than those between Au_4 and $Au_9(SR)_6$ cage in $Au_{21}(SR)_{15}$, which shows the weaker aurophilic interaction in $Au_{22}(SR)_{16}$ over that in $Au_{21}(SR)_{15}$. This also suggests the less thermostability of $Au_{22}(SR)_{16}$ than $Au_{21}(SR)_{15}$.

Structural prediction of more stable isomers of $Au_{22}(SR)_{16}$

Based on the Ring model, we have obtained the structural insights into the less thermostability of $Au_{22}(SAdm)_{16}$

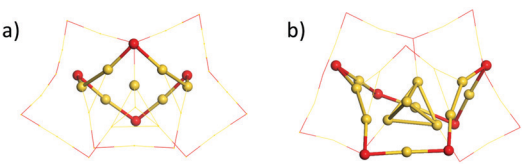

Fig. 3 The structure locates at the centre of (a) the $[Au_6(SR)_4]$ ring in the $Au_{21}(SR)_{15}$ cluster and (b) the $[Au_8(SR)_6]$ ring in the $Au_{22}(SR)_{16}$ cluster. Au: yellow; S: red. The R groups are omitted for clarity.

Table 1 Inner structure of $Au_9(SR)_6$ cage in $Au_{21}(SR)_{15}$ and $Au_{10}(SR)_7$ cage in $Au_{22}(SR)_{16}$ *via* the Ring model

	$[Au_5(SR)_3]$	$[Au_6(SR)_4]$	$[Au_7(SR)_5]$	$[Au_8(SR)_6]$
$Au_9(SR)_6$ cage	Au	Au	Au_4	—
$Au_{10}(SR)_7$ cage	Au	—	Au_4	Au_4
Ring model	Au	Au/Au_4	Au_4	$2Au_4$

Table 2 The average distance between the gold atoms in tetrahedral Au_4 and the gold atoms of the surrounded rings. d_1, d_2 and d_3 denote the average distance between the gold atoms in tetrahedral Au_4 and the gold atoms of $[Au_7(SR)_5]$, $[Au_6(SR)_4]$, and $[Au_5(SR)_3]$ rings in the $Au_9(SR)_6$ cage in $Au_{21}(SR)_{15}$, respectively. d_1^*, d_2^* and d_3^* denote the average distances between the gold atoms in tetrahedral Au_4 and the gold atoms of $[Au_8(SR)_6]$, $[Au_7(SR)_5]$, and $[Au_5(SR)_3]$ rings in the $Au_9(SR)_6$ cage in $Au_{21}(SR)_{15}$, respectively. R is simplified as CH_3

$Au_{21}(SR)_{15}$			$Au_{22}(SR)_{16}$		
d_1 (Å)	d_2 (Å)	d_3 (Å)	d_1^* (Å)	d_2^* (Å)	d_3^* (Å)
2.980	3.030	2.762	3.368	3.223	2.949

compared with $Au_{21}(SR)_{15}$, one may question if there exist more stable isomers of $Au_{22}(SR)_{16}$ with respect to the available crystallized structure (referred as Iso1 hereafter).

Recently, the GUM and Ring model have been used widely to predict the atomic structures of thiolate-protected gold nanoclusters, *i.e.*, $Au_{28+4n}(SR)_{20+2n}$ (n = 0–8) nanoclusters and $Au_{15}(SR)_{13}$ nanocluster with a new type of ligand $[Au_7(SR)_7]$ ring.[29,30] Here, the GUM together with the Ring model was employed to the structural predictions for $Au_{22}(SR)_{16}$. Based on GUM, two new Au_{11} and Au_{10} cores can be constructed by three packing or fusing tetrahedral Au_4 units, as shown in Fig. 4. The Au_{11} core can be viewed as one bi-tetrahedron Au_7 and one tetrahedron Au_4 packing together, while the Au_{10} core can be viewed as three tetrahedron Au_4 fusing together by sharing two gold atoms. Then, in accordance with the Ring model, the outer ligands were added to protect the newly constructed cores. For the Au_{11} core, two $Au(SR)_2$, one $Au_2(SR)_3$, one $Au_3(SR)_4$, and one $Au_4(SR)_5$ ligands were added to surround the Au_{11} core *via* the formation of two $[Au_4(SR)_2]$, one $[Au_4(SR)_3]$, one $[Au_6(SR)_4]$, and one $[Au_6(SR)_5]$ rings (filled with green color in Fig. 4), which ultimately forms the whole structure of a new $Au_{22}(SR)_{16}$ isomer (referred as Iso2 hereafter). Following the same way, two $Au(SR)_2$, two $Au_2(SR)_3$, and one $Au_6(SR)_6$ ligands can be added on the Au_{10} core *via* the formation of two $[Au_4(SR)_2]$, one $[Au_4(SR)_3]$, one $[Au_6(SR)_3]$, and one $[Au_6(SR)_6]$ rings (filled with green color in Fig. 4) to form the whole structure of another new $Au_{22}(SR)_{16}$ isomer (referred as Iso3). It should be noted that the $[Au_6(SR)_6]$ ring has been confirmed in crystallized $Au_{28}(SR)_{22}$ nanoclusters.[31]

Further analysis on three $Au_{22}(SR)_{18}$ isomers *via* density functional theory calculations

To show the advantages of these two newly constructed isomers, density functional theory (DFT) calculations were performed to obtain the electronic properties of three $Au_{22}(SR)_{16}$ isomers with the Perdew–Burke–Ernzerhof (PBE) functional and the all-electron basis set 6-31G(d) for C, H, and S, pseudopotential basis set LANL2DZ for Au. In addition, Tao–Perdew–Staroverov–Scuseria functional (TPSS) and Becke's three parameter hybrid functional with the Lee–Yang–Parr correlation functional (B3LYP) were also employed to check the stabilities of $Au_{22}(SR)_{16}$ isomers. $-CH_3$ was used as the outer organic ligand. All calculations were performed using the Orca package.[32] Super-fast approximate TD-DFT implemented in the Orca package by Grimme *et al.* was used to obtain the UV-abs spectrum.[33] As shown in Table 3, calculations using the three functionals (PBE, TPSS, and B3LYP) confirmed that both Iso2 and Iso3 had lower relative energies and larger HOMO–LUMO gaps (HL gaps) than the crystallized Iso1 with R = CH_3.

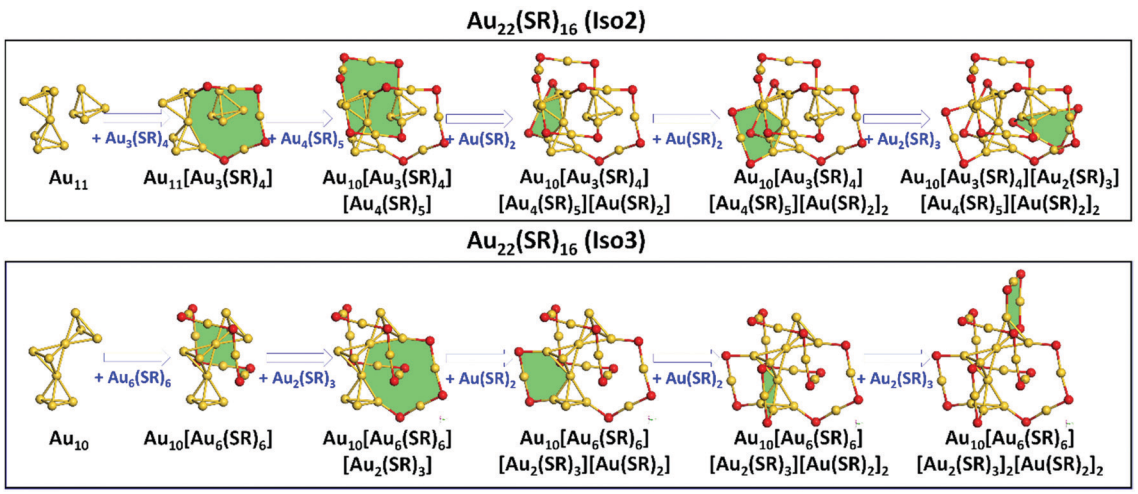

Fig. 4 The structural predictions of two $Au_{22}(SR)_{16}$ isomers Iso2 (upper panel) and Iso3 (lower panel). Au: yellow; S: red. The rings were filled with green color. The R groups are omitted for clarity.

Table 3 Relative energies and HOMO–LUMO gaps of three $Au_{22}(SR)_{16}$ (R = CH_3) isomers

	Relative energy (eV)			HOMO–LUMO gap (eV)		
$Au_{22}(SR)_{16}$	PBE	TPSS	B3LYP	PBE	TPSS	B3LYP
Iso1	0.30	0.25	0.21	1.66	1.59	2.75
Iso2	0.17	0.18	0.03	1.90	1.79	3.20
Iso3	0.00	0.00	0.00	1.97	1.96	3.20

Frequency calculations showed that no imagination frequency existed, which confirmed the stability of these clusters. Calculations using the PBE functional showed that Iso2 was more stable than Iso1 by 0.17 eV, while Iso3 showed further stability with respect to Iso1 by 0.30 eV, which suggested the high stabilities of the predicted Iso2 and Iso3. Similar to the relative energy, taking the PBE functional as an example, Iso2 and Iso3 showed greater HOMO–LUMO gaps by 0.24 and 0.31 eV over Iso1, respectively. All the three functionals showed that Iso3 had the lowest relative energy and the largest HOMO–LUMO gap.

The calculated absorption spectra of the three $Au_{22}(SR)_{16}$ isomers are presented to compare with the experimental measurement and to obtain the optical absorption properties of the predicted isomers. PBE functional is widely known to cause a red-shift in the spectrum;[34] herein, CAM-B3LYP was used to get the absorption spectra. Gaussian broadening was applied in obtaining the absorption spectra using the reorganization energy (Fig. S1, ESI†) as widths. It can be seen in Fig. 5 that the prominent absorption peaks of Iso1 (2.10, 2.53 eV) could well reproduce the experimental peaks (2.04, 2.66 eV), indicating the reliabilities of the theoretical methods employed in our simulations. In addition, the main absorption peak for Iso2 was 2.70 eV. Two absorption peaks for Iso3 included 2.81 eV and 2.97 eV.

To show the optical emission properties of the three isomers, results on photoemission are also presented here, as can be seen in Fig. 6. Experimentally, Iso1 yielded emission at 1.60 eV from its first excited state. Fig. 6 and Fig. S1 (ESI†) showed that calculations using PBE functional gave 1.23 eV,

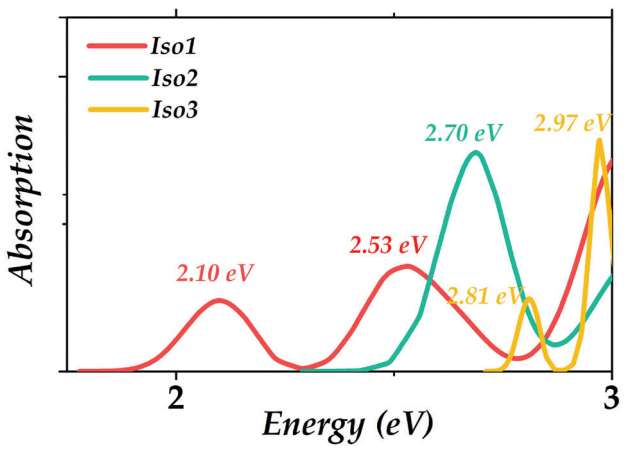

Fig. 5 Calculated optical absorption spectra for the three $Au_{22}(SR)_{16}$ (R = CH_3) isomers.

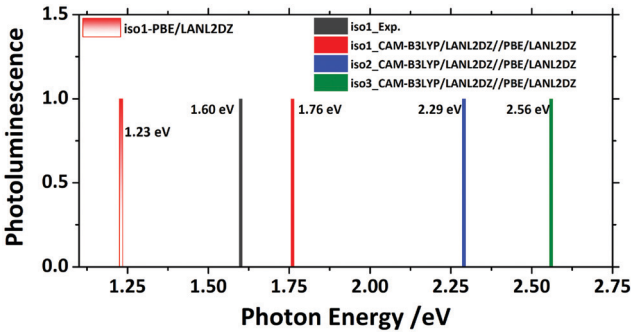

Fig. 6 Photoluminescence spectra of the three $Au_{22}(SR)_{16}$ (R = CH_3) isomers.

which was significantly lower than the experimental one due to the lack of exact exchange.[34] Thus, CAM-B3LYP functional was also used to rectify the emission spectrum, resulting in the emission peak (1.76 eV) that had a good agreement with the experiment (1.60 eV). Calculations showed that the emission peaks from the first excited state of Iso2 and Iso3 were 2.29 eV and 2.56 eV, respectively.

Conclusions

In summary, based on the recently developed Ring model, we presented new structural insights into the lower thermostability of $Au_{22}(SAdm)_{16}$ than $Au_{21}(SAdm)_{15}$. The violation of the Ring Model for the rings in $Au_{22}(SAdm)_{16}$ as well as the weaker aurophilic interactions between the Au_4 core and surrounded rings in $Au_{22}(SAdm)_{16}$ led to the spontaneous transformation from $Au_{22}(SAdm)_{16}$ to $Au_{21}(SAdm)_{15}$. Further, with GUM and the Ring model, another two new $Au_{22}(SR)_{16}$ isomers with lower relative energies and higher HOMO–LUMO gaps over the crystallized isomer were predicted.

Conflicts of interest

There are no conflicts to declare.

Acknowledgements

W. W. X. was supported by Natural Science Foundation of China (Grant No. 11974195). E. W. thanks for the open fund of the state key laboratory of molecular reaction dynamics in DICP, CAS (SKLMRD-K202201).

References

1 R. Jin, C. Zeng, M. Zhou and Y. Chen, *Chem. Rev.*, 2016, **116**, 10346–10413.
2 Z. Ma, P. Wang, L. Xiong and Y. Pei, *WIREs Comput. Mol. Sci.*, 2017, 7, e1315.
3 W. W. Xu, X. C. Zeng and Y. Gao, *Acc. Chem. Res.*, 2018, **51**, 2739–2747.
4 E. Wang and Y. Gao, *J. Chem. Phys.*, 2021, **155**, 044302.

5 X. Kang, Y. Li, M. Zhu and R. Jin, *Chem. Soc. Rev.*, 2020, **49**, 6443–6514.
6 X. Kang and M. Zhu, *Chem. Soc. Rev.*, 2019, **48**, 2422–2457.
7 X. Kang and M. Zhu, *Chem. Mater.*, 2021, **33**, 39–62.
8 X. Liu, W. W. Xu, X. Huang, E. Wang, X. Cai, Y. Zhao, J. Li, M. Xiao, C. Zhang, Y. Gao, W. Ding and Y. Zhu, *Nat. Commun.*, 2020, **11**, 3349.
9 S. Tian, Y.-Z. Li, M.-B. Li, J. Yuan, J. Yang, Z. Wu and R. Jin, *Nat. Commun.*, 2015, **6**, 8667.
10 L. Liao, S. Zhuang, C. Yao, N. Yan, J. Chen, C. Wang, N. Xia, X. Liu, M.-B. Li, L. Li, X. Bao and Z. Wu, *J. Am. Chem. Soc.*, 2016, **138**, 10425–10428.
11 Q. Li, S. Yang, T. Chen, S. Jin, J. Chai, H. Zhang and M. Zhu, *Nanoscale*, 2020, **12**, 23694–23699.
12 S. Chen, L. Xiong, S. Wang, Z. Ma, S. Jin, H. Sheng, Y. Pei and M. Zhu, *J. Am. Chem. Soc.*, 2016, **138**, 10754–10757.
13 H. Häkkinen, M. Walter and H. Grönbeck, *J. Phys. Chem. B*, 2006, **110**, 9927–9931.
14 D.-e Jiang, M. L. Tiago, W. Luo and S. Dai, *J. Am. Chem. Soc.*, 2008, **130**, 2777–2779.
15 C. M. Aikens, *Acc. Chem. Res.*, 2018, **51**, 3065–3073.
16 T. Higaki, Q. Li, M. Zhou, S. Zhao, Y. Li, S. Li and R. Jin, *Acc. Chem. Res.*, 2018, **51**, 2764–2773.
17 Q. Tang, G. Hu, V. Fung and D.-E. Jiang, *Acc. Chem. Res.*, 2018, **51**, 2793–2802.
18 K. L. D. M. Weerawardene, H. Häkkinen and C. M. Aikens, *Annu. Rev. Phys. Chem.*, 2018, **69**, 205–229.
19 P. Chakraborty, A. Nag, A. Chakraborty and T. Pradeep, *Acc. Chem. Res.*, 2019, **52**, 2–11.
20 Y. Pei, P. Wang, Z. Ma and L. Xiong, *Acc. Chem. Res.*, 2019, **52**, 23–33.
21 M. Walter, J. Akola, O. Lopez-Acevedo, P. D. Jadzinsky, G. Calero, C. J. Ackerson, R. L. Whetten, H. Grönbeck and H. Häkkinen, *Proc. Natl. Acad. Sci. U. S. A.*, 2008, **105**, 9157.
22 L. Cheng, Y. Yuan, X. Zhang and J. Yang, *Angew. Chem., Int. Ed.*, 2013, **52**, 9035–9039.
23 L. Cheng, C. Ren, X. Zhang and J. Yang, *Nanoscale*, 2013, **5**, 1475–1478.
24 A. Tlahuice-Flores, *J. Phys. Chem. C*, 2019, **123**, 10831–10841.
25 Y. Pei, P. Wang, Z. Ma and L. Xiong, *Acc. Chem. Res.*, 2019, **52**, 23–33.
26 W. W. Xu, B. Zhu, X. C. Zeng and Y. Gao, *Nat. Commun.*, 2016, **7**, 13574.
27 W. Han, P. Liu, M. Zheng, X. C. Zeng and W. W. Xu, *J. Phys. Chem. Lett.*, 2021, **12**, 3006–3013.
28 L. Yang, Q. He, W. Han, P. Liu and W. W. Xu, *Chem. Phys. Lett.*, 2021, **785**, 139133.
29 P. Liu, W. Han, M. Zheng, W. Li, J. Ren, A. Tlahuice-Flores and W. W. Xu, *J. Phys. Chem. A*, 2021, **125**, 5933–5938.
30 P. Liu, W. Han, M. Zheng and W. W. Xu, *Nanoscale*, 2020, **12**, 20677–20683.
31 Y. G. Srinivasulu, N. Goswami, Q. Yao and J. Xie, *J. Phys. Chem. C*, 2021, **125**, 4066–4076.
32 F. Neese, F. Wennmohs, U. Becker and C. Riplinger, *J. Chem. Phys.*, 2020, **152**, 224108.
33 M. de Wergifosse and S. Grimme, *J. Chem. Phys.*, 2018, **149**, 024108.
34 M. J. Alhilaly, M. S. Bootharaju, C. P. Joshi, T. M. Besong, A.-H. Emwas, R. Juarez-Mosqueda, S. Kaappa, S. Malola, K. Adil, A. Shkurenko, H. Häkkinen, M. Eddaoudi and O. M. Bakr, *J. Am. Chem. Soc.*, 2016, **138**, 14727–14732.

